Asociación Argentina
de Mecánica Computacional

Mecánica Computacional Vol XXIX, págs. 4105-4126 (artículo completo)
Eduardo Dvorkin, Marcela Goldschmit, Mario Storti (Eds.)
Buenos Aires, Argentina, 15-18 Noviembre 2010

A STUDY ON NONLINEAR STRESS AND STRAIN FIELDS IN TWO-DIMENSIONAL PANELS OF ELASTIC COMPOSITE MATERIALS

Clayton T. Aquino, Severino P. C. Marques and Eduardo N. Lages

Laboratório de Computação Científica e Visualização, Centro de Tecnologia, Universidade Federal de Alagoas. Campus A. C. Simões – 57072-970 – Maceió- AL, http://www.lccv.ufal.br

Keywords: Finite-Volume Theory, geometrical nonlinearity, heterogeneous materials.

Abstract. This work presents a study on strain and stress distributions in two-dimensional panels constituted by elastic composite materials considering effects of physical and geometrical nonlinearities. The analyses are carried out by a new nonlinear model which is based on the parametric finite-volume theory. The model is incremental and uses a total Lagragian formulation that employs the Second Piola-Kirchhoff tensor and Green-Lagrange tensor as stress and strain measurements, respectively. The composite material and its constituents are assumed as linear or nonlinear elastic. The analyzed examples include two-dimensional panels with circular and elliptic inclusions presenting a large range of mismatch ratios for their Young's moduli. In particular, stress concentrations in panels of functionally graded materials with circular and elliptic holes are analyzed. The study presents the distributions of stresses and strains over the matrices and inclusions of the composite materials. Results obtained by finite element method are also used for comparison.

1 INTRODUCTION

Due to the technological importance of the advanced composite materials, many studies have been developed to understand the behavior of them under different loading conditions and, consequently, to improve the project procedures and their industrial applications. Among these advanced materials are the fiber reinforced composites consisting of high performance fibers embedded in a matrix and exhibiting high specific stiffness/strength as relevant features. Other important class of advanced composites is constituted by the functionally graded materials (FGMs). These later materials are new composites that present a graded microstructure obtained by gradual variations of the volume fractions of their constituent phases.

The heterogeneous microstructures of such composites are responsible for a more complex mechanical behavior in comparison with that exhibited by the traditional homogeneous materials. Computational tools for the analysis of the mechanical behavior of composites demand larger processing times and, often, require the employ of especial numerical techniques. For complicated geometries, or in the presence of nonlinear effects, for which the problem cannot be tackled using analytical solutions, the finite element method has emerged as the more employed numerical approach for the description of the composite mechanical behavior.

An attractive alternative for the analysis of structural problem involving heterogeneous materials is the finite-volume theory. Based on this framework, the well-known Finite-Volume Direct Averaging Micromechanics – FVDAM was formulated to the thermomechanical analysis of composite materials (Bansal and Pindera, 2003). The standard FVDAM employs rectangular subvolumes to mimic structural components with heterogeneous microstructure. This imposes limitations on the efficiency of the theory to model structural components that present curved boundaries or microstructure constituted by inclusions with curved cross sections. These limitations have been overcome by the recently developed parametric formulation of FVDAM (Cavalcante, 2006; Cavalcante et al. 2007a, b). This new formulation employs quadrilateral subvolumes for the microstructural discretization of a structural component what has allowed a much more efficient and accurate modeling of problem with arbitrarily-shaped external boundary or microstructure exhibiting inclusions with arbitrary cross sections.

This work presents a study on strains and stresses in panels constituted by elastic composite materials, using a two-dimensional nonlinear parametric finite-volume formulation presented in Aquino (2010) and based on the linear model initially developed by Cavalcante (2006). The formulation is incremental and uses a total Lagrangian kinematic description. The material is considered as elastic and the displacements are assumed as arbitrarily large. As measures of stress and strain, the formulation employs the 2nd Piola-Kirchhoff stress tensor and Green-Lagrange strain tensor, respectively (Bathe, 1996). To verify the performance of the formulation, the results are compared with solutions obtained by finite element method.

2 THE NONLINEAR PARAMETRIC FINITE-VOLUME FORMULATION

2.1 Local coordinate transformation

Similar to the finite element method and linear parametric formulation of finite-volume theory, the geometrically nonlinear formulation requires a generation of a mesh constituted by subvolumes. The position and geometry of each subvolume are defined by its four vertices and faces as illustrated in Figure 1.

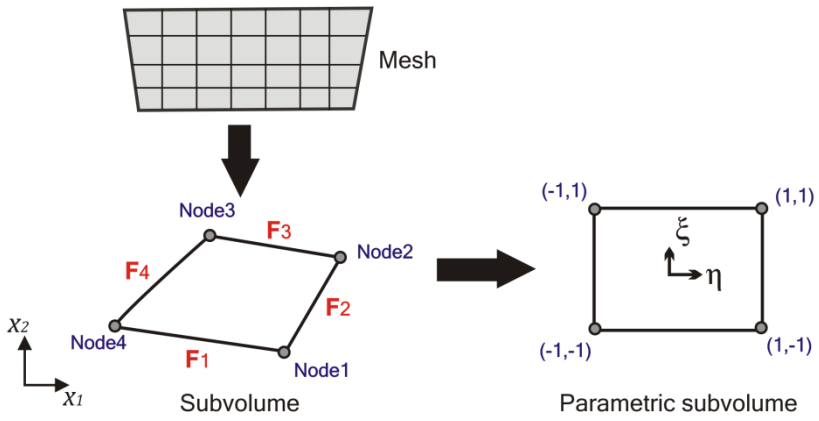

Figure 1: Mesh and parametric subvolume.

The mapping of the point (η, ξ) in the reference subvolume to the corresponding point (X_1, X_2) in the subvolume of the actual discretization is given by

$$X_i(\eta,\xi) = N_1(\eta,\xi)X_i^{nó1} + N_2(\eta,\xi)X_i^{nó2} + N_3(\eta,\xi)X_i^{nó3} + N_4(\eta,\xi)X_i^{nó4} \tag{1}$$

where

$$\begin{aligned} N_1(\eta,\xi) &= \frac{1}{4}(1-\eta)(1-\xi) \\ N_2(\eta,\xi) &= \frac{1}{4}(1+\eta)(1-\xi) \\ N_3(\eta,\xi) &= \frac{1}{4}(1+\eta)(1+\xi) \\ N_4(\eta,\xi) &= \frac{1}{4}(1-\eta)(1+\xi) \end{aligned} \tag{2}$$

The derivatives of the displacement field ${}^t u$ with respect to the parametric coordinates are given by the following expressions

$$\begin{aligned} \frac{\partial\ {}^t u_i}{\partial \eta} &= \frac{\partial\ {}^t u_i}{\partial X_j}\frac{\partial X_j}{\partial \eta} \\ \frac{\partial\ {}^t u_i}{\partial \xi} &= \frac{\partial\ {}^t u_i}{\partial X_j}\frac{\partial X_j}{\partial \xi} \end{aligned} \tag{3}$$

or, in matrix notation, in the form,

$$\begin{Bmatrix} \frac{\partial\ {}^{t}u_i}{\partial\eta} \\ \frac{\partial\ {}^{t}u_i}{\partial\xi} \end{Bmatrix} = \begin{bmatrix} \frac{\partial X_1}{\partial\eta} & \frac{\partial X_2}{\partial\eta} \\ \frac{\partial X_1}{\partial\xi} & \frac{\partial X_2}{\partial\xi} \end{bmatrix} \begin{Bmatrix} \frac{\partial\ {}^{t}u_i}{\partial X_1} \\ \frac{\partial\ {}^{t}u_i}{\partial X_2} \end{Bmatrix} \tag{4}$$

In Equation (4), the derivatives of the actual coordinates with respect to the parametric coordinates are the components of the Jacobian matrix $\boldsymbol{J}$:

$$\boldsymbol{J} = \begin{bmatrix} \frac{\partial X_1}{\partial\eta} & \frac{\partial X_2}{\partial\eta} \\ \frac{\partial X_1}{\partial\xi} & \frac{\partial X_2}{\partial\xi} \end{bmatrix} = \begin{bmatrix} i_1 + i_2\xi & i_4 + i_5\xi \\ i_3 + i_2\eta & i_6 + i_5\eta \end{bmatrix} \tag{5}$$

where

$$\begin{Bmatrix} i_1 \\ i_2 \\ i_3 \end{Bmatrix} = \frac{1}{4}\begin{bmatrix} -1 & 1 & 1 & -1 \\ 1 & -1 & 1 & -1 \\ -1 & -1 & 1 & 1 \end{bmatrix} \begin{Bmatrix} X_1^{node1} \\ X_1^{node2} \\ X_1^{node3} \\ X_1^{node4} \end{Bmatrix} \tag{6}$$

$$\begin{Bmatrix} i_4 \\ i_5 \\ i_6 \end{Bmatrix} = \frac{1}{4}\begin{bmatrix} -1 & 1 & 1 & -1 \\ 1 & -1 & 1 & -1 \\ -1 & -1 & 1 & 1 \end{bmatrix} \begin{Bmatrix} X_2^{node1} \\ X_2^{node2} \\ X_2^{node3} \\ X_2^{node4} \end{Bmatrix} \tag{7}$$

In the present formulation, by reason of simplification, the Jacobian matrix is considered constant for each subvolume and given by

$$\boldsymbol{J} \approx \begin{bmatrix} i_1 & i_4 \\ i_3 & i_6 \end{bmatrix} \tag{8}$$

Hence, the inverse of the Jacobian matrix for each subvolume can be writen as follows:

$$\boldsymbol{J}^{-1} \approx \bar{\boldsymbol{J}} = \frac{1}{i_7}\begin{bmatrix} i_6 & -i_4 \\ -i_3 & i_1 \end{bmatrix} \tag{9}$$

where

$$i_7 = i_1\, i_6 - i_3 i_4 \tag{10}$$

Using the Equations (4) and (9), the following expression can be

$$\begin{Bmatrix} \frac{\partial\ {}^{t}\bar{u}_1}{\partial X_1} \\ \frac{\partial\ {}^{t}\bar{u}_1}{\partial X_2} \\ \frac{\partial\ {}^{t}\bar{u}_2}{\partial X_1} \\ \frac{\partial\ {}^{t}\bar{u}_2}{\partial X_2} \end{Bmatrix} = \bar{\mathcal{J}} \begin{Bmatrix} \frac{\partial\ {}^{t}\bar{u}_1}{\partial \eta} \\ \frac{\partial\ {}^{t}\bar{u}_1}{\partial \xi} \\ \frac{\partial\ {}^{t}\bar{u}_2}{\partial \eta} \\ \frac{\partial\ {}^{t}\bar{u}_2}{\partial \xi} \end{Bmatrix} \tag{11}$$

being

$$\bar{\mathcal{J}} = \begin{bmatrix} \bar{J} & \mathbf{0} \\ \mathbf{0} & \bar{J} \end{bmatrix} \tag{12}$$

where $\mathbf{0}$ is a null square matrix with the same order of $\bar{J}$.

2.2 Approximation of the displacement field

Figure 2 shows the motion of a subvolume in the Cartesian coordinate system defined by the axes x_1 e x_2 through the equilibrium configurations ${}^{0}\mathcal{C}$, ${}^{t}\mathcal{C}$ e ${}^{t+\Delta t}\mathcal{C}$, corresponding to the times t_0, t e $t+\Delta t$, respectivamente.

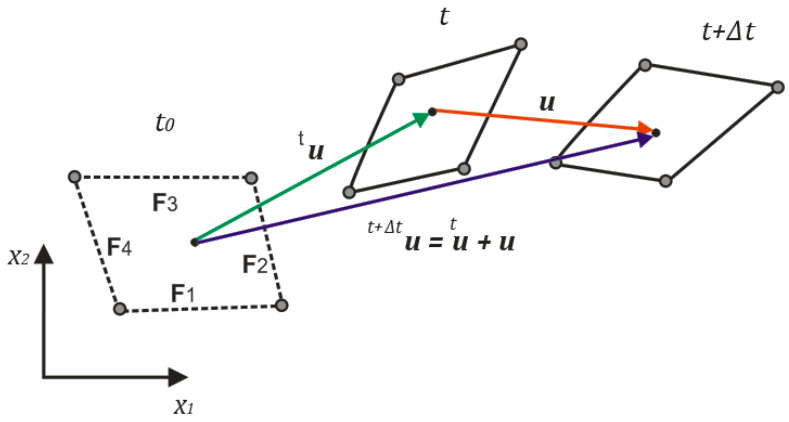

Figure 2: Motion of a subvolume in the Cartesian coordinate system.

The displacement fields of the subvolume in a general configuration are approximated by the following quadratic expansions:

$${}^{t}u_i = {}^{t}U_{i(00)} + \eta\ {}^{t}U_{i(10)} + \xi\ {}^{t}U_{i(01)} + \frac{1}{2}(3\eta^2 - 1)\ {}^{t}U_{i(20)} + \frac{1}{2}(3\xi^2 - 1)\ {}^{t}U_{i(02)} \tag{13}$$

whereas the increments in the displacement fields are given

$$u_i = U_{i(00)} + \eta U_{i(10)} + \xi U_{i(01)} + \frac{1}{2}(3\eta^2 - 1)U_{i(20)} + \frac{1}{2}(3\xi^2 - 1)U_{i(02)} \tag{14}$$

In the Equations (13) and (14), the symbols ${}^{t}U_{i(..)}$ and $U_{i(..)}$ indicate the coefficients of the polynomial expansions. During the incremental procedure, for the analysis of the equilibrium configuration ${}^{t+\Delta t}\mathcal{C}$, it is supposed that the coefficients corresponding to the configuration ${}^{t}\mathcal{C}$ are known.

Using the incremental relation ${}^{t+\Delta t}u = {}^{t}u + u$, the following expression can be easily derived

$$ {}^{t+\Delta t}U_{i(mn)} = {}^{t}U_{i(mn)} + U_{i(mn)} \tag{15} $$

2.3 Incremental equations of continuum mechanics

The incremental constitutive equation of a material can be written in the form

$$ \boldsymbol{S} = \boldsymbol{C}\boldsymbol{E} \tag{16} $$

where $\boldsymbol{S}$ and $\boldsymbol{E}$ stand for, respectively, the increments of the 2nd Piola-Kirchhoff stress tensor and of the Green-Lagrange strain tensor and $\boldsymbol{C}$ indicates the elastic constitutive tensor of the material.

The increment of the traction vector associated with the tensor $\boldsymbol{S}$ is given by Cauchy's stress theorem, as follows:

$$ \boldsymbol{T} = \boldsymbol{S}^{T}\,\boldsymbol{N} \tag{17} $$

being $\boldsymbol{N}$ the unit outward normal vector referred to the initial configuration.

The following decompositions can be derived involving the stress tensor and the traction vector corresponding to the configurations ${}^{t}\mathcal{C}$ and ${}^{t+\Delta t}\mathcal{C}$

$$ {}^{t+\Delta t}\boldsymbol{S} = {}^{t}\boldsymbol{S} + \boldsymbol{S} \tag{18} $$

$$ {}^{t+\Delta t}\boldsymbol{T} = {}^{t}\boldsymbol{T} + \boldsymbol{T} \tag{19} $$

Neglecting the nonlinear part in the increment of the Green-Lagrange strain tensor, the incremental Equation (16) can be written in terms of surface-averaged values as follows:

$$\begin{Bmatrix} \bar{S}_{11} \\ \bar{S}_{22} \\ \bar{S}_{12} \end{Bmatrix}_{\eta=\pm 1} = \begin{bmatrix} C_{11} & C_{12} & 0 \\ C_{21} & C_{22} & 0 \\ 0 & 0 & C_{33} \end{bmatrix} \begin{Bmatrix} \bar{\epsilon}_{11} \\ \bar{\epsilon}_{22} \\ \bar{\epsilon}_{12} \end{Bmatrix}_{\eta=\pm 1} \tag{20}$$

$$\begin{Bmatrix} \bar{S}_{11} \\ \bar{S}_{22} \\ \bar{S}_{12} \end{Bmatrix}_{\xi=\pm 1} = \begin{bmatrix} C_{11} & C_{12} & 0 \\ C_{21} & C_{22} & 0 \\ 0 & 0 & C_{33} \end{bmatrix} \begin{Bmatrix} \bar{\epsilon}_{11} \\ \bar{\epsilon}_{22} \\ \bar{\epsilon}_{12} \end{Bmatrix}_{\xi=\pm 1} \tag{21}$$

where the bar is used to indicate average value on the subvolume faces.

Hence, the surface-averaged 2nd Piola-Kirchhoff stress tensor on each face and corresponding to the configuration ${}^{t+\Delta t}\mathcal{C}$ can be given in the form

$${}^{t+\Delta t}\bar{\boldsymbol{S}}_{\eta=\pm 1} = {}^{t}\bar{\boldsymbol{S}}_{\eta=\pm 1} + \boldsymbol{C}\left(\boldsymbol{E}_l + \boldsymbol{E}_g\, {}^{t}\boldsymbol{H}_{\eta=\pm 1}\right)\bar{\boldsymbol{J}}\, \boldsymbol{G}_{\eta=\pm 1}\boldsymbol{U} \tag{22}$$

$${}^{t+\Delta t}\bar{\boldsymbol{S}}_{\xi=\pm 1} = {}^{t}\bar{\boldsymbol{S}}_{\xi=\pm 1} + \boldsymbol{C}\left(\boldsymbol{E}_l + \boldsymbol{E}_g\, {}^{t}\boldsymbol{H}_{\xi=\pm 1}\right)\bar{\boldsymbol{J}}\, \boldsymbol{G}_{\xi=\pm 1}\boldsymbol{U} \tag{23}$$

where $\boldsymbol{U}$ is the vector of coefficients of the incremental displacement field with transpose
$U^{tr} = \{U_{1(00)} \quad U_{1(10)} \quad U_{1(01)} \quad U_{1(20)} \quad U_{1(02)}\}$. The matrices E_l, E_g, ${}^{t}H$, G e G are presented in the Appendix A.

Equation (17) can be written in terms of surface-averaged values on the faces in the following form:

Face 1-3:

$$\begin{Bmatrix} {}^{t+\Delta t}\bar{T}_1^{(k)} \\ {}^{t+\Delta t}\bar{T}_2^{(k)} \end{Bmatrix} = \begin{bmatrix} N_1^{(k)} & 0 & N_2^{(k)} \\ 0 & N_2^{(k)} & N_1^{(k)} \end{bmatrix} \begin{Bmatrix} {}^{t+\Delta t}\bar{S}_{11} \\ {}^{t+\Delta t}\bar{S}_{22} \\ {}^{t+\Delta t}\bar{S}_{12} \end{Bmatrix}_{\xi=\pm 1} \tag{24}$$

Face 2-4:

$$\begin{Bmatrix} {}^{t+\Delta t}\bar{T}_1^{(k)} \\ {}^{t+\Delta t}\bar{T}_2^{(k)} \end{Bmatrix} = \begin{bmatrix} N_1^{(k)} & 0 & N_2^{(k)} \\ 0 & N_2^{(k)} & N_1^{(k)} \end{bmatrix} \begin{Bmatrix} {}^{t+\Delta t}\bar{S}_{11} \\ {}^{t+\Delta t}\bar{S}_{22} \\ {}^{t+\Delta t}\bar{S}_{12} \end{Bmatrix}_{\eta=\pm 1} \tag{25}$$

where ${}^{t+\Delta t}\bar{T}_1^{(k)}$ and ${}^{t+\Delta t}\bar{T}_2^{(k)}$ are the components of the average 2nd Piola-Kirchhoff traction vector for the face k and configuration ${}^{t+\Delta t}\mathcal{C}$.

Equations (24) and (25) can be written together by the expression

$$\begin{Bmatrix} {}^{t+\Delta t}\bar{T}_1^{(1)} \\ {}^{t+\Delta t}\bar{T}_2^{(1)} \\ {}^{t+\Delta t}\bar{T}_1^{(2)} \\ {}^{t+\Delta t}\bar{T}_2^{(2)} \\ {}^{t+\Delta t}\bar{T}_1^{(3)} \\ {}^{t+\Delta t}\bar{T}_2^{(3)} \\ {}^{t+\Delta t}\bar{T}_1^{(4)} \\ {}^{t+\Delta t}\bar{T}_2^{(4)} \end{Bmatrix} = \begin{bmatrix} \boldsymbol{N}^{(1)} & \mathbf{0} & \mathbf{0} & \mathbf{0} \\ \mathbf{0} & \boldsymbol{N}^{(2)} & \mathbf{0} & \mathbf{0} \\ \mathbf{0} & \mathbf{0} & \boldsymbol{N}^{(3)} & \mathbf{0} \\ \mathbf{0} & \mathbf{0} & \mathbf{0} & \boldsymbol{N}^{(4)} \end{bmatrix} \begin{Bmatrix} {}^{t+\Delta t}\bar{S}_{\xi=-1} \\ {}^{t+\Delta t}\bar{S}_{\eta=+1} \\ {}^{t+\Delta t}\bar{S}_{\xi=+1} \\ {}^{t+\Delta t}\bar{S}_{\eta=-1} \end{Bmatrix} \tag{26}$$

Substituting the Equations (22) and (23) into Equation (26), the following expression involving the average 2nd Piola-Kirchhoff traction vector and the coefficients of the incremental displacement field can be found:

$${}^{t+\Delta t}\bar{\boldsymbol{T}} = \mathbb{N}\ {}^{t}\bar{\boldsymbol{S}} + \mathbb{N}\,\mathbb{C}\left(\mathbb{E}_l + \mathbb{E}_g\ {}^{t}\mathbb{H}\right)\bar{\mathbb{J}}\,\mathbb{G}\,\boldsymbol{U} \tag{27}$$

being the matrices $\mathbb{N}$, $\mathbb{C}$, $\mathbb{E}_l$, $\mathbb{E}_g$, ${}^{t}\mathbb{H}$, $\bar{\mathbb{J}}$ and $\mathbb{G}$ presented in Appendix A. From Equations (19) and (27), the following expressions can be written

$${}^{t}\bar{\boldsymbol{T}} = \mathbb{N}\ {}^{t}\bar{\boldsymbol{S}} \tag{28}$$

$$\bar{\boldsymbol{T}} = \mathbb{N}\,\mathbb{C}\left(\mathbb{E}_l + \mathbb{E}_g\ {}^{t}\mathbb{H}\right)\bar{\mathbb{J}}\,\mathbb{G}\,\boldsymbol{U} \tag{29}$$

2.4 Local equilibrium equations

Figure 3 shows a subvolume in the configuration ${}^{t+\Delta t}\mathcal{C}$ subjected to the average first Piola-Kirchhoff tractions ${}^{t+\Delta t}\bar{\boldsymbol{T}}^{(k)}$ and body forces b_v.

The equilibrium equations for the subvolume can be written in the form

$$\sum_{k=1}^{4} {}^{t+\Delta t}\bar{T}_i^{(k)} A_k + b_{vi} = 0 \tag{30}$$

where A_k indicates the area of kth subvolume face.

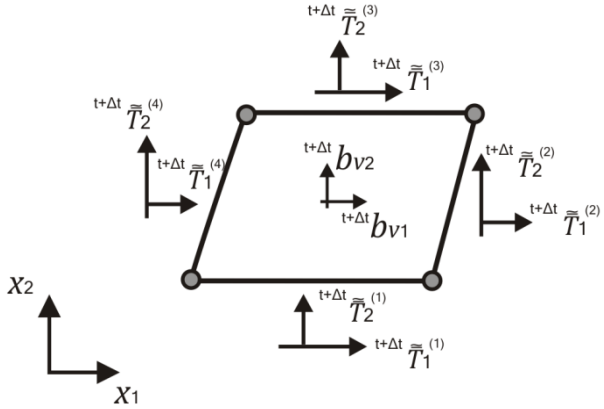

Figure 3: Piola-Kirchhoff tractions and body forces in a subvolume.

Supposing that the strain gradient tensor of the subvolume is constant and given by

$$ {}^{t+\Delta t}\bar{\bar{F}} = \begin{bmatrix} 1 & 0 \\ 0 & 1 \end{bmatrix} + \begin{bmatrix} \dfrac{\partial {}^{t+\Delta t}\bar{u}_1}{\partial X_1} & \dfrac{\partial {}^{t+\Delta t}\bar{u}_1}{\partial X_2} \\ \dfrac{\partial {}^{t+\Delta t}\bar{u}_2}{\partial X_1} & \dfrac{\partial {}^{t+\Delta t}\bar{u}_2}{\partial X_2} \end{bmatrix} \tag{31} $$

the following equation involving the tractions of the first Piola-Kirchhoff and 2nd Piola-Kirchhoff vectors is obtained:

$$ {}^{t+\Delta t}\bar{\bar{T}}^{(k)} \cong {}^{t+\Delta t}\bar{\bar{F}} \;\; {}^{t+\Delta t}\bar{\bar{T}}^{(k)} \tag{32} $$

Using the Equations (32) and (30), it is possible to obtain the expression that connects the coefficients of the incremental displacement field to the surface-averaged incremental displacements $u_{i_{Fj}}$ as follows

$$ \begin{Bmatrix} U_{1(10)} \\ U_{1(01)} \\ U_{1(20)} \\ U_{1(02)} \\ U_{2(10)} \\ U_{2(01)} \\ U_{2(20)} \\ U_{2(02)} \end{Bmatrix} = \frac{1}{2}\boldsymbol{M} - \boldsymbol{L}\,\boldsymbol{\Phi}^{-1}\boldsymbol{\Theta}\boldsymbol{M} \begin{Bmatrix} u_{1_{F1}} \\ u_{2_{F1}} \\ u_{1_{F2}} \\ u_{2_{F2}} \\ u_{1_{F3}} \\ u_{2_{F3}} \\ u_{1_{F4}} \\ u_{2_{F4}} \end{Bmatrix} - \boldsymbol{L}\,\boldsymbol{\Phi}^{-1}\boldsymbol{\Omega} \tag{33} $$

where the matrices $\boldsymbol{L}$, $\boldsymbol{\Phi}$, $\boldsymbol{\Theta}$, $\boldsymbol{M}$ e $\boldsymbol{\Omega}$ are presented in Appendix A.
Considering the Equation (33) in (29), the incremental expression relating the surface-averaged tractions and displacements on the subvolume faces becomes

$$ \bar{\bar{T}} = \boldsymbol{K}\,\boldsymbol{u}_F - \boldsymbol{f}_v \tag{34} $$

where

$$\boldsymbol{u}_F^{tr} = \{u_{1_{F1}} \quad u_{2_{F1}} \quad u_{1_{F2}} \quad u_{2_{F2}} \quad u_{1_{F3}} \quad u_{2_{F3}} \quad u_{1_{F4}} \quad u_{2_{F4}}\} \tag{35}$$

$$\boldsymbol{K} = \left(\boldsymbol{\mathcal{F}}\left(\mathbb{A} + {}^{t}\mathbb{B}\right) + \boldsymbol{\mathcal{T}}\boldsymbol{\mathcal{S}}\right)\left(\boldsymbol{P} - \boldsymbol{L}\,\boldsymbol{\Phi}^{-1}\boldsymbol{\Theta}\boldsymbol{M}\right) \tag{36}$$

$$\boldsymbol{f}_v = \left(\boldsymbol{\mathcal{F}}\left(\mathbb{A} + {}^{t}\mathbb{B}\right) + \boldsymbol{\mathcal{T}}\boldsymbol{\mathcal{S}}\right)\left(\mathbb{A} + {}^{t}\mathbb{B}\right)\boldsymbol{L}\,\boldsymbol{\Phi}^{-1}\boldsymbol{\Omega} \tag{37}$$

$\boldsymbol{K}$ represent the subvolume stiffness matrices and $\boldsymbol{f}_v$ is a vector of pseudo-stresses dependent on the increments of the body forces.

The global incremental equation that relates increments of surface-averaged displacements $\mathbb{U}$ to increments of surface-averaged tractions $\mathbb{T}$ of the discretized model is obtained through the contribution of each subvolume using Equation (34) and interfacial compatibility conditions involving surface-averaged values of increments of displacements and tractions. This global incremental equation is given by

$$\mathbb{T} = \mathbb{K}\,\mathbb{U} - \mathbb{F}_v \tag{38}$$

where $\mathbb{K}$ and $\mathbb{F}_v$ are the global incremental stiffness matrix of the structure and the global incremental pseudo-stress vector, respectively.

3 INCREMENTAL NONLINEAR ELASTIC CONSTITUTIVE RELATION

The incremental nonlinear elastic constitutive relationship used in this work is derived in terms of the secant bulk K_s and shear moduli G_s which are assumed as functions of the infinitesimal octahedral strains ε_{oct} and γ_{oct}, as follows:

$$\begin{aligned} K_s &= K_s(\varepsilon_{oct}) \\ G_s &= G_s(\gamma_{oct}) \end{aligned} \tag{39}$$

Differentiation of the secant octahedral stress-strain relations yields the following expressions for the tangent bulk and shear moduli, respectively,

$$\begin{aligned} K_t &= K_s + \varepsilon_{oct}\frac{dK_s}{d\varepsilon_{oct}} \\ G_t &= G_s + \gamma_{oct}\frac{dG_s}{d\gamma_{oct}} \end{aligned} \tag{40}$$

Hence, considering the relationships between the increments of total and octahedral stresses and strains, the terms of the incremental tangent stiffness matrix ***C*** appearing in Equation (16) can be derived as

$$C_{ij} = 2\left[\left(\frac{K_t}{2} - \frac{G_s}{3}\right)\delta_{ij}\delta_{kl} + G_s\delta_{ik}\delta_{jl} + \eta\epsilon_{ij}\epsilon_{kl}\right] \tag{41}$$

where $\eta = \frac{4}{3}\frac{(G_t - G_s)}{\gamma_{oct}^2}$. The symbols δ and ϵ indicate the Kronecker delta and infinitesimal total strain, respectively.

4 NUMERICAL EXAMPLES

4.1 Circular fiber embedded in a large matrix

This example treats of a circular fiber immersed in a large matrix subjected to uniform far-field tensile loading σ along the horizontal direction as shown in Figure 4. For the case of infinity matrix, this problem consists of a particular case of the well-known Eshelby problem (Eshelby, 1957). Here, the fiber diameter and the matrix side were assumed as being $\mathrm{D} = 2\ \mathrm{cm}$ and $\mathrm{L} = 20\ \mathrm{cm}$, respectively.

Due to the symmetry of the structure, only one-quarter of the domain was modeled, using 376 subvolumes (Figure 5). In the two initial cases, the materials were assumed as linear elastic with the properties showed in Table 1. The results are showed in Figures 6 and 7.

Figure 6 presents the variation of the Cauchy normal stress with the mean horizontal displacement on the loaded end face. As observed, the results obtained by the presented formulation (FVT) are in an excellent agreement with those corresponding to the analytical solution and finite element method (FEM).

Figure 7 shows the results for the case 2. The normal stresses in the fiber and matrix were obtained on the centers of the subvolumes near the fiber-matrix interface showed in Figure 5. The results corresponding to the FVT and FEM are in a very good agreement.

Table 1: Material elastic properties of the inclusion problem.

Case	***Material***	$E(GPa)$	ν
1	Fiber	10	0.25
	Matrix	10	0.25
2	Fiberglass	64	0.20
	Matrix Epoxy	4.8	0.34

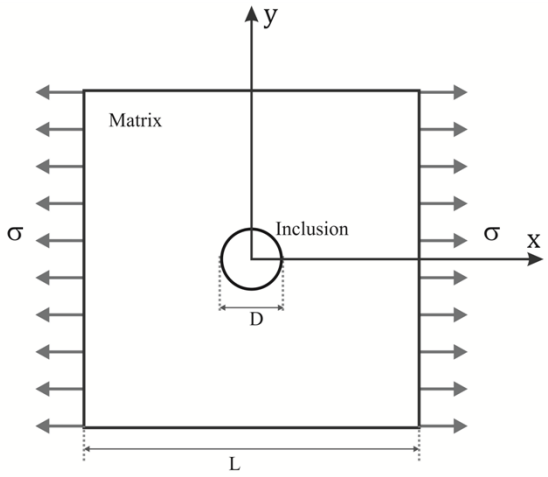

Figure 4: Circular fiber inside a large matrix.

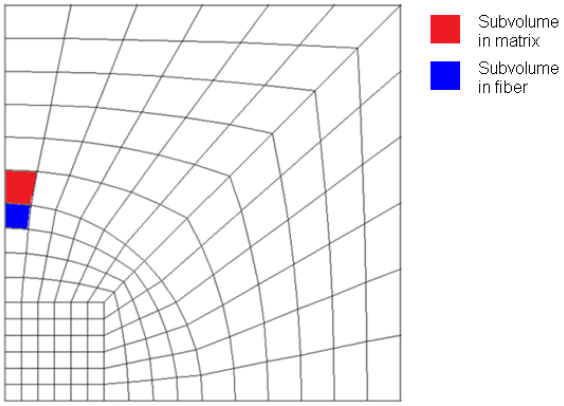

Figure 5: Discretization near the inclusion region.

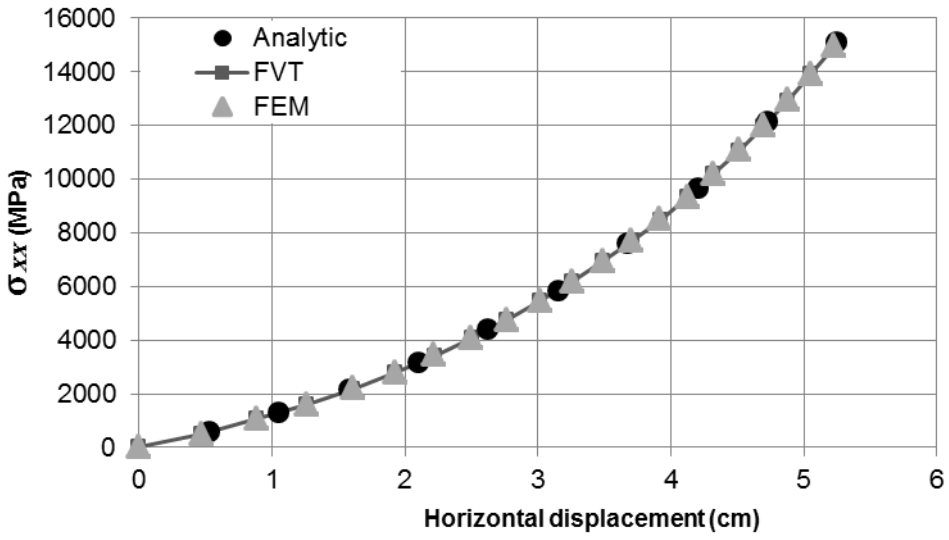

Figure 6: Normal stress σ_{xx} in function of the horizontal displacement for case 1.

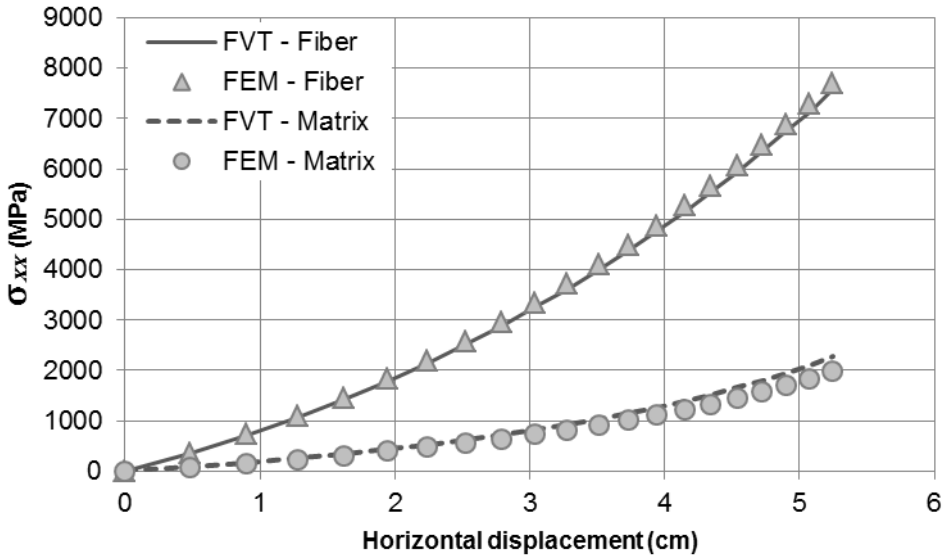

Figure 7: Normal stress σ_{xx} in function of the horizontal displacement for case 2.

In this last case, the elastic linear fiber is embedded in a nonlinear elastic matrix whose properties are presented in Table 2. The secant bulk modulus of the matrix K_s is assumed as constant and the relation between the octahedral shear stress and the associated octahedral shear strain is given by

$$\tau_{oct} = \tau_{op}\left[1 - exp\left(-\frac{G_0}{\tau_{op}}\gamma_{oct}\right)\right] \tag{42}$$

Figure 8 shows the results of τ_{oct} in function of the mean horizontal displacement on the end loaded face. The change of curvature observed in Figure 8 can be explained by the increasing material nonlinear effect with the displacement.

Table 2: Material properties of the inclusion problem.

Material	$E(GPa)$	ν	τ_{op}	G_0
Fiber	64	0.20	-	-
Matrix	4.8	0.34	5000	974.921

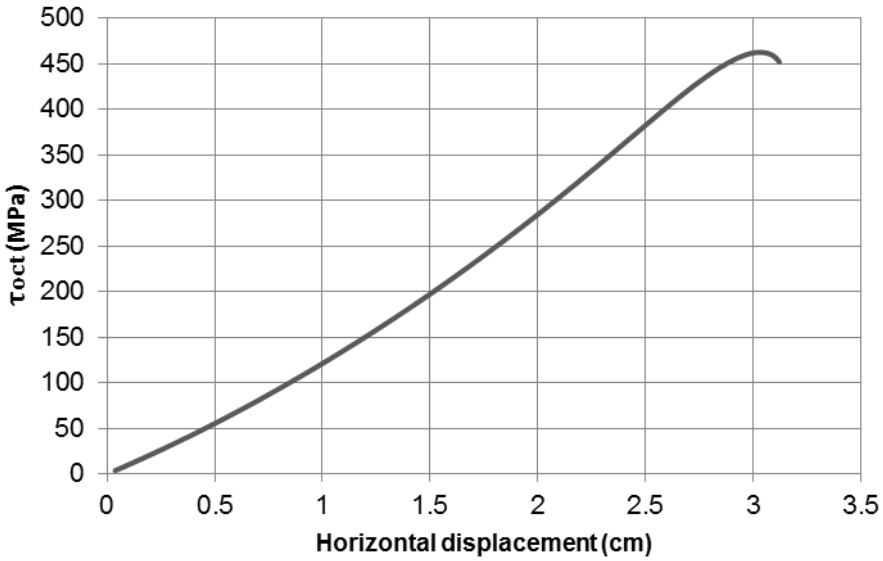

Figure 8: Variation of τ_{oct} with the horizontal displacement for nonlinear elastic matrix.

4.2 Stress concentration in a panel of FGM with a circular hole

This example present a study on stress concentration around a circular hole in a panel made of a functionally graded material subjected to a tensile loading, as showed in Figure 9. The material is assumed as isotropic and linear elastic, exhibiting a gradation for the Young's modulus defined by the law

$$E_{fgm}(y) = \left[1 - \left(\frac{y}{10}\right)^p\right] E_c + \left(\frac{y}{10}\right)^p E_m \tag{43}$$

where E_c and E_m stand for Young's moduli of the ceramic (Zirconia) and metal (NiCoCrAlY) phases, respectively. p indicates the gradation parameter. The panel is square with side $L = 20\ cm$ and the hole has a diameter $D = 2\ cm$. Table 3 shows the elastic properties of the phases.

Table 3 – Material elastic properties – FGM panel.

Material	$E(GPa)$	ν
Ceramic (Zirconia)	70	0.24
Metal (NiCoCrAlY)	170	0.24

Figure 10 presents the discretization used to model one-quarter of the panel. The normal stress σ_{xx} is obtained on the point $A\ (\mathrm{x} = 0.025\ m; \mathrm{y} = 1.025\ m)$ showed in Figure 9.

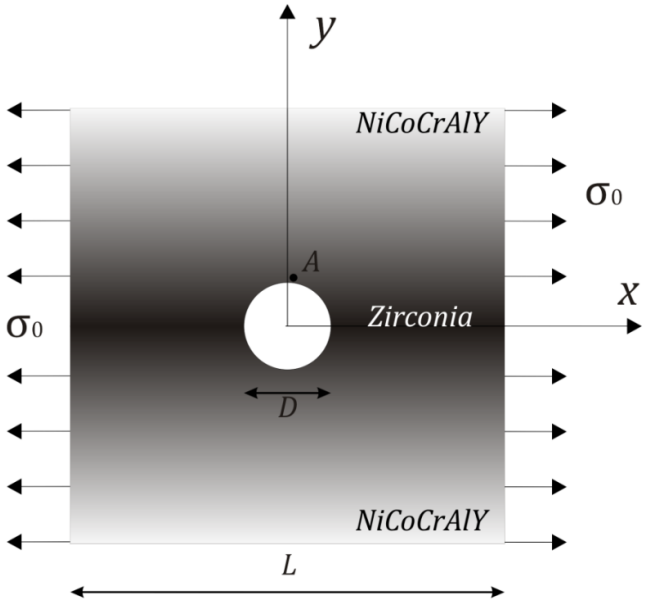

Figure 9: FGM panel with a central hole.

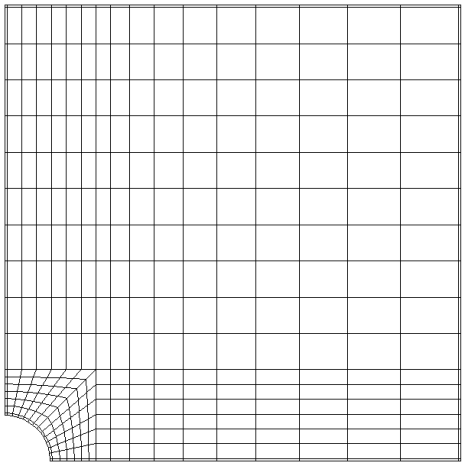

Figure 10: Discretization of one-quarter of the FGM panel (373 subvolumes).

Figures 11 and 12 show, respectively, the variations of the normal stress in the point A and the associated stress concentration factor $SCF = \frac{\sigma_{xx}}{\sigma_0}$ in function of the horizontal displacement in the point ($x = 10\ m; y = 0$) for $p = 0$. The results obtained by the present formulation and finite element method are close. As expected, $SCF \approx 3$ for small displacements, in agreement with the linear fracture mechanics theory.

Figures 13 and 14 present the same results for the case $p = 0.5$. As observed, the FVT and FEM provide close results, particularly for the range of small displacements. As observed in Figure 14, the values of the SCF are reduced by the material gradation.

Figure 15 shows the variation of the SCF in function of the gradation parameter p together with results obtained by Santos Júnior et al. (2009) using graded finite elements.

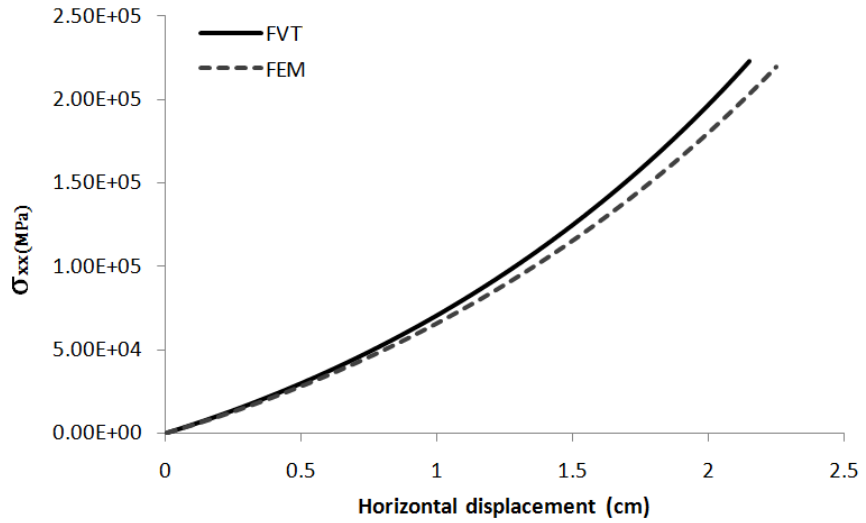

Figure 11: Variation of the normal stress in A with the horizontal displacement for $p = 0$.

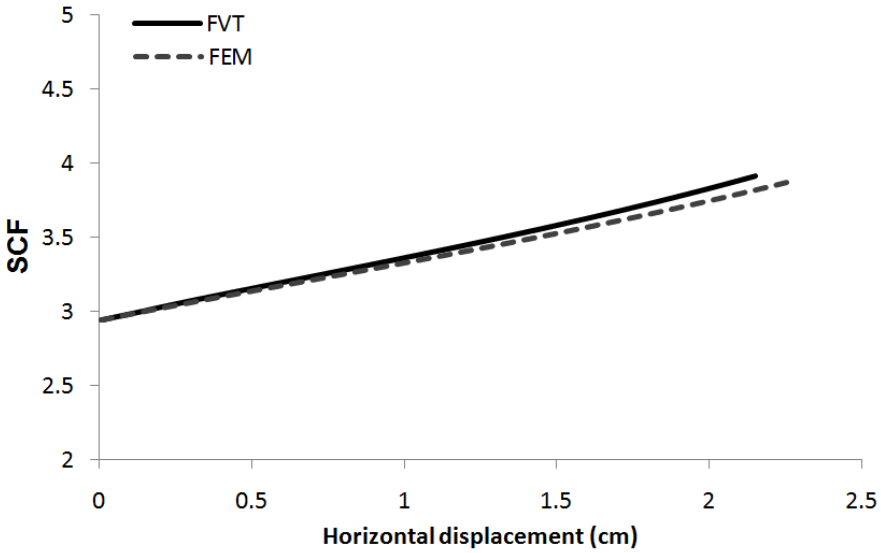

Figure 12: Variation of the SCF with the horizontal displacement for $p = 0$.

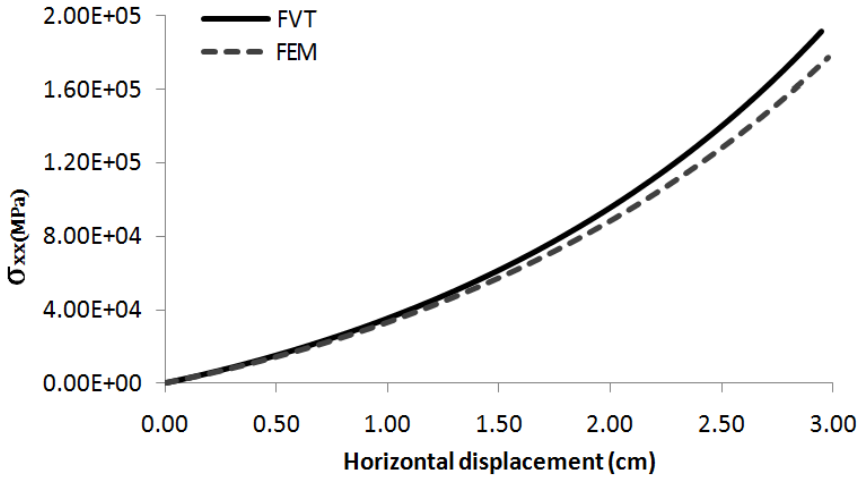

Figure 13: Variation of the normal stress in A with the horizontal displacement for $p = 0.5$.

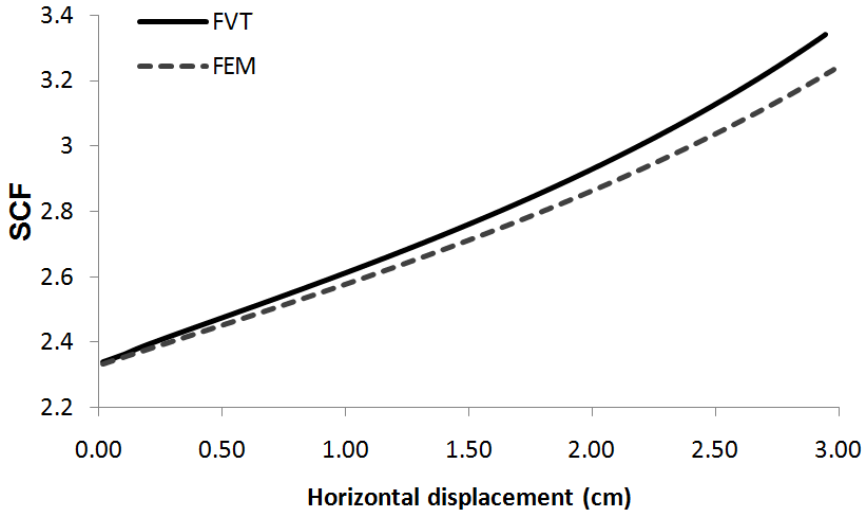

Figure 14: Variation of the SCF with the horizontal displacement for $p = 0.5$.

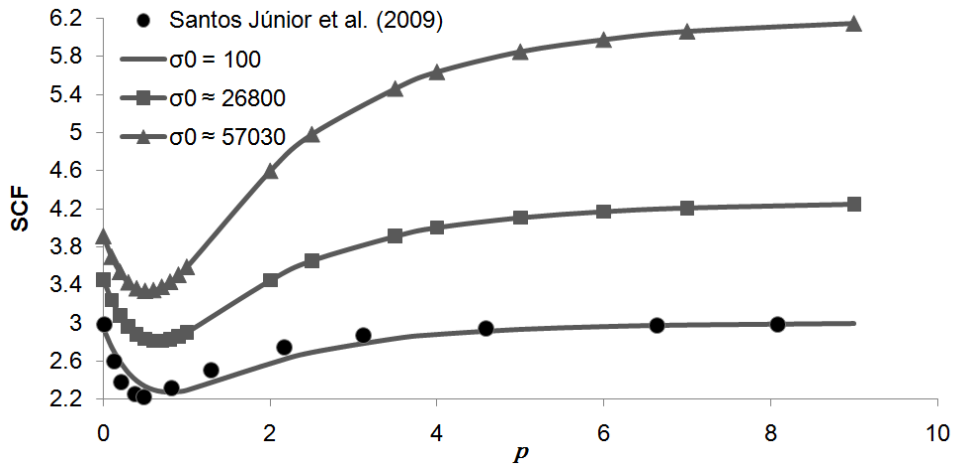

Figure 15: Variation of the SCF with the parameter p.

5 CONCLUSIONS

A two-dimensional nonlinear parametric formulation for the mechanical analysis of structures made of elastic heterogeneous materials has been presented and applied to the analysis of stresses and strains in composite panels. The model is incremental and based on the linear parametric formulation of FVDAM. A total Lagragian kinematic description is utilized by the formulation. The first analyzed example consists of a panel constituted by a circular linear elastic fiber embedded in a large matrix subjected to a tensile loading. For this example, the matrix has been considered as constituted by linear and nonlinear elastic materials. The second analyzed case consists of an FGM panel with a central circular hole under a tensile loading. For this example, the stress concentration around the hole has been studied. The results have been compared with others determined through a code based on the finite element method, exhibiting a very good agreement.

Acknowledgements

The authors would like to gratefully acknowledge the support of the Laboratory of Scientific Computation and Visualization (LCCV) and Brazilian federal agencies CAPES and CNPq.

REFERENCES

Aquino, C. T. (2010). Uma Formulação Geometricamente não Linear da Teoria Paramétrica de Volumes Finitos. Dissertação de Mestrado. Programa de Pós-Graduação em Engenharia Civil – UFAL.

Bansal, Y. and Pindera, M-J. (2003). Efficient reformulation of the thermoelastic higher order theory for FGMs. *Journal of Thermal Stresses*, v.26(11/12), p. 1055-1092.

Bathe, K. J. (1996). Finite Element Procedures, Prentice Hall, Englewood-Cliffs.

Cavalcante, M. A. A. (2006). Modelagem do Comportamento Termo-Mecânico Transiente de Estruturas de Materiais Compósitos pela Teoria de Volumes Finitos. Dissertação de Mestrado. Programa de Pós-Graduação em Engenharia Civil – UFAL.

Cavalcante, M. A. A.; Marques, S. P. C.; Pindera, M. J. (2007a). Parametric Formulation of the Finite-Volume Theory for Functionally Graded Materials—Part I: Analysis. *Journal of Applied Mechanics*, v. 74, p. 935-945.

Cavalcante, M. A. A.; Marques, S. P. C.; Pindera, M. J. (2007b). Parametric Formulation of the Finite-Volume Theory for Functionally Graded Materials—Part II: Numerical Results. *Journal of Applied Mechanics*, v. 74, p. 946-957.

Eshelby, J. D. (1957) The determination of the Elastic Field of an ellipsoidal Inclusion and Related Problems. *Proceedings of the Royal Society*, v.A241, p. 376-396.

Santos Júnior, A.; Marques, S. P. C; Cavalcante, M. A. A. (2009) A Study on Stress Concentration Around Circular Hole in Panel of Functionally Graded. *XXX CILAMCE - Iberian Latin-American Congress on Computational Methods in Engineering*.

APPENDIX

$$\mathbb{C} = \begin{bmatrix} \boldsymbol{C} & \boldsymbol{0} & \boldsymbol{0} & \boldsymbol{0} \\ \boldsymbol{0} & \boldsymbol{C} & \boldsymbol{0} & \boldsymbol{0} \\ \boldsymbol{0} & \boldsymbol{0} & \boldsymbol{C} & \boldsymbol{0} \\ \boldsymbol{0} & \boldsymbol{0} & \boldsymbol{0} & \boldsymbol{C} \end{bmatrix} \tag{44}$$

$$\mathbb{N} = \begin{bmatrix} \boldsymbol{N^{(1)}} & \boldsymbol{0} & \boldsymbol{0} & \boldsymbol{0} \\ \boldsymbol{0} & \boldsymbol{N^{(2)}} & \boldsymbol{0} & \boldsymbol{0} \\ \boldsymbol{0} & \boldsymbol{0} & \boldsymbol{N^{(3)}} & \boldsymbol{0} \\ \boldsymbol{0} & \boldsymbol{0} & \boldsymbol{0} & \boldsymbol{N^{(4)}} \end{bmatrix} \tag{45}$$

$$\mathbb{E}_l = \begin{bmatrix} \boldsymbol{E_l} & \boldsymbol{0} & \boldsymbol{0} & \boldsymbol{0} \\ \boldsymbol{0} & \boldsymbol{E_l} & \boldsymbol{0} & \boldsymbol{0} \\ \boldsymbol{0} & \boldsymbol{0} & \boldsymbol{E_l} & \boldsymbol{0} \\ \boldsymbol{0} & \boldsymbol{0} & \boldsymbol{0} & \boldsymbol{E_l} \end{bmatrix} \tag{46}$$

$$\mathbb{E}_g = \begin{bmatrix} \boldsymbol{E_g} & \boldsymbol{0} & \boldsymbol{0} & \boldsymbol{0} \\ \boldsymbol{0} & \boldsymbol{E_g} & \boldsymbol{0} & \boldsymbol{0} \\ \boldsymbol{0} & \boldsymbol{0} & \boldsymbol{E_g} & \boldsymbol{0} \\ \boldsymbol{0} & \boldsymbol{0} & \boldsymbol{0} & \boldsymbol{E_g} \end{bmatrix} \tag{47}$$

$$\bar{\mathbb{J}} = \begin{bmatrix} \boldsymbol{\bar{J}} & \boldsymbol{0} & \boldsymbol{0} & \boldsymbol{0} & \boldsymbol{0} & \boldsymbol{0} & \boldsymbol{0} & \boldsymbol{0} \\ \boldsymbol{0} & \boldsymbol{\bar{J}} & \boldsymbol{0} & \boldsymbol{0} & \boldsymbol{0} & \boldsymbol{0} & \boldsymbol{0} & \boldsymbol{0} \\ \boldsymbol{0} & \boldsymbol{0} & \boldsymbol{\bar{J}} & \boldsymbol{0} & \boldsymbol{0} & \boldsymbol{0} & \boldsymbol{0} & \boldsymbol{0} \\ \boldsymbol{0} & \boldsymbol{0} & \boldsymbol{0} & \boldsymbol{\bar{J}} & \boldsymbol{0} & \boldsymbol{0} & \boldsymbol{0} & \boldsymbol{0} \\ \boldsymbol{0} & \boldsymbol{0} & \boldsymbol{0} & \boldsymbol{0} & \boldsymbol{\bar{J}} & \boldsymbol{0} & \boldsymbol{0} & \boldsymbol{0} \\ \boldsymbol{0} & \boldsymbol{0} & \boldsymbol{0} & \boldsymbol{0} & \boldsymbol{0} & \boldsymbol{\bar{J}} & \boldsymbol{0} & \boldsymbol{0} \\ \boldsymbol{0} & \boldsymbol{0} & \boldsymbol{0} & \boldsymbol{0} & \boldsymbol{0} & \boldsymbol{0} & \boldsymbol{\bar{J}} & \boldsymbol{0} \\ \boldsymbol{0} & \boldsymbol{0} & \boldsymbol{0} & \boldsymbol{0} & \boldsymbol{0} & \boldsymbol{0} & \boldsymbol{0} & \boldsymbol{\bar{J}} \end{bmatrix} \tag{48}$$

$$\mathbb{G} = \begin{bmatrix} \boldsymbol{G_{\xi=-1}} \\ \boldsymbol{G_{\eta=+1}} \\ \boldsymbol{G_{\xi=+1}} \\ \boldsymbol{G_{\eta=-1}} \end{bmatrix} \tag{49}$$

$$\boldsymbol{G_{\eta=\pm1}} = \begin{bmatrix} 1 & 0 & 3\eta & 0 & 0 & 0 & 0 & 0 \\ 0 & 1 & 0 & 0 & 0 & 0 & 0 & 0 \\ 0 & 0 & 0 & 0 & 1 & 0 & 3\eta & 0 \\ 0 & 0 & 0 & 0 & 0 & 1 & 0 & 0 \end{bmatrix} \tag{50}$$

$$\boldsymbol{G_{\xi=\pm1}} = \begin{bmatrix} 1 & 0 & 0 & 0 & 0 & 0 & 0 & 0 \\ 0 & 1 & 0 & 3\xi & 0 & 0 & 0 & 0 \\ 0 & 0 & 0 & 0 & 1 & 0 & 0 & 0 \\ 0 & 0 & 0 & 0 & 0 & 1 & 0 & 3\xi \end{bmatrix} \tag{51}$$

$$\boldsymbol{L}^{tr} = \begin{bmatrix} 0 & 0 & 0 & 0 & 0 & 0 & 1 & 1 \\ 0 & 0 & 1 & 1 & 0 & 0 & 0 & 0 \end{bmatrix} \tag{52}$$

$${}^{t}\mathbb{H} = \begin{bmatrix} {}^{t}\boldsymbol{H}_{\xi=-1} & \mathbf{0} & \mathbf{0} & \mathbf{0} \\ \mathbf{0} & {}^{t}\boldsymbol{H}_{\eta=+1} & \mathbf{0} & \mathbf{0} \\ \mathbf{0} & \mathbf{0} & {}^{t}\boldsymbol{H}_{\xi=+1} & \mathbf{0} \\ \mathbf{0} & \mathbf{0} & \mathbf{0} & {}^{t}\boldsymbol{H}_{\eta=-1} \end{bmatrix} \tag{53}$$

$${}^{t}\boldsymbol{H}_{\substack{\eta=\pm1 \\ \xi=\pm1}} = \begin{bmatrix} \frac{\partial\ {}^{t}\bar{u}_1}{\partial X_1} & 0 & \frac{\partial\ {}^{t}\bar{u}_2}{\partial X} & 0 \\ 0 & \frac{\partial\ {}^{t}\bar{u}_1}{\partial X_2} & 0 & \frac{\partial\ {}^{t}\bar{u}_2}{\partial X_2} \\ 0 & \frac{\partial\ {}^{t}\bar{u}_1}{\partial X_1} & 0 & \frac{\partial\ {}^{t}\bar{u}_2}{\partial X_1} \\ \frac{\partial\ {}^{t}\bar{u}_1}{\partial X_2} & 0 & \frac{\partial\ {}^{t}\bar{u}_2}{\partial X_2} & 0 \end{bmatrix}_{\substack{\eta=\pm1 \\ \xi=\pm1}} \tag{54}$$

$$\boldsymbol{M} = \begin{bmatrix} 0 & 0 & 1 & 0 & 0 & 0 & -1 & 0 \\ -1 & 0 & 0 & 0 & 1 & 0 & 0 & 0 \\ 0 & 0 & 1 & 0 & 0 & 0 & 1 & 0 \\ 1 & 0 & 0 & 0 & 1 & 0 & 0 & 0 \\ 0 & 0 & 0 & 1 & 0 & 0 & 0 & -1 \\ 0 & -1 & 0 & 0 & 0 & 1 & 0 & 0 \\ 0 & 0 & 0 & 1 & 0 & 0 & 0 & 1 \\ 0 & 1 & 0 & 0 & 0 & 1 & 0 & 0 \end{bmatrix} \tag{55}$$

$$\boldsymbol{\Theta} = \frac{1}{2}\ {}^{t}\boldsymbol{D} \tag{56}$$

$$\boldsymbol{\Phi} = \begin{bmatrix} \mathrm{D}_{13} + \mathrm{D}_{14} & \mathrm{D}_{17} + \mathrm{D}_{18} \\ \mathrm{D}_{23} + \mathrm{D}_{24} & \mathrm{D}_{27} + \mathrm{D}_{28} \end{bmatrix} \tag{57}$$

$$\boldsymbol{\Omega} = \begin{Bmatrix} b_{v1} \\ b_{v2} \end{Bmatrix} \tag{58}$$

$${}^{t}\boldsymbol{D} = \left(\boldsymbol{I} + {}^{t}\boldsymbol{V}\right)\boldsymbol{A}\left(\mathbb{A} + {}^{t}\mathbb{B}\right) + {}^{t}\mathbb{X} \tag{59}$$

$${}^{t}\mathbb{X} = c_1 \begin{bmatrix} J_{11} & J_{12} & 0 & 0 & 0 & 0 & 0 & 0 \\ 0 & 0 & 0 & 0 & J_{11} & J_{12} & 0 & 0 \end{bmatrix} + c_2 \begin{bmatrix} J_{21} & J_{22} & 0 & 0 & 0 & 0 & 0 & 0 \\ 0 & 0 & 0 & 0 & J_{21} & J_{22} & 0 & 0 \end{bmatrix} \tag{60}$$

where

$$c_i = \sum_{k=1}^{4} A_k \; {}^{t}\bar{T}_i^{(k)} \tag{61}$$

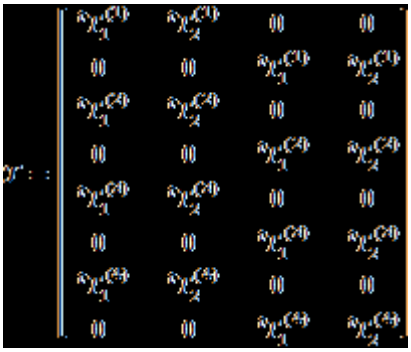

(62)

$$\boldsymbol{S} = \begin{bmatrix} \bar{J}_{11} & \bar{J}_{12} & 0 & 0 & 0 & 0 & 0 & 0 \\ \bar{J}_{21} & \bar{J}_{22} & 0 & 0 & 0 & 0 & 0 & 0 \\ 0 & 0 & 0 & 0 & \bar{J}_{11} & \bar{J}_{12} & 0 & 0 \\ 0 & 0 & 0 & 0 & \bar{J}_{21} & \bar{J}_{22} & 0 & 0 \end{bmatrix} \tag{63}$$